1 Relative Humidity Effect on the Formation of Highly Oxidized Molecules and

2 New Particles during Monoterpene Oxidation

- 3 Xiaoxiao Li^{1,2}, Sabrina Chee¹, Jiming Hao², Jonathan P. D. Abbatt³, Jingkun Jiang^{2*}, and James N.
- 4 Smith^{1*}
- 5 ¹Chemistry Department, University of California, Irvine, CA 92697, USA
- ²State Key Joint Laboratory of Environment Simulation and Pollution Control, School of Environment, Tsinghua University,
- 7 Beijing, 100084, China
- 8 ³Department of Chemistry, University of Toronto, Toronto, Canada
- 9 *: Correspondence to: J. N. Smith (jimsmith@uci.edu) and J. Jiang (jiangjk@tsinghua.edu.cn)
- 10 **Abstract.** It has been widely observed around the world that the frequency and intensity of new particle formation (NPF) 11 events are reduced during periods of high relative humidity (RH). The current study focuses on how RH affects the formation 12 of highly oxidized molecules (HOMs), which are key components of NPF and initial growth caused by oxidized organics. The 13 ozonolysis of α -pinene, limonene, and Δ^3 -carene, with and without OH-scavenger, were carried out under low NOx conditions 14 under a range of RH (from ~3% to ~92%) in a temperature-controlled flow tube to generate secondary organic aerosol (SOA). 15 A Scanning Mobility Particle Sizer (SMPS) was used to measure the size distribution of generated particles and a novel 16 transverse-ionization chemical ionization inlet with a high-resolution time-of-fight mass spectrometer detected HOMs. A 17 major finding from this work is that neither the detected HOMs nor their abundance changed significantly with RH, which 18 indicates that the detected HOMs must be formed from water-independent pathways. In fact, the distinguished OH- and 19 O₃-derived peroxy radicals (RO₂), HOM monomers, and HOM dimers could mostly be explained by the autoxidation of RO₂ 20 followed by bimolecular reactions with other RO₂ or hydroperoxy radicals (HO₂), rather than from a water-influenced pathway 21 like through the formation of a stabilized Criegee intermediate (sCI). However, as RH increased from ~3% to ~92%, the total 22 SOA number concentrations decreased by a factor of 2-3 while SOA mass concentrations remains relatively constant. These 23 observations show that, while high RH appears to inhibit NPF as evident by the decreasing number concentration, this 24 reduction is not caused by a decrease in RO₂-derived HOM formation. Possible explanations to these phenomena were 25 discussed.

1 Introduction

26

27

28

29

30

New particle formation (NPF) is ubiquitous around the world (Kulmala et al., 2004). Newly formed particles contribute greatly to global particle populations and can grow further to act as cloud condensation nuclei (CCN), thereby influencing clouds and climate (Makkonen et al., 2012; Merikanto et al., 2009; Dunne et al., 2016). NPF characteristics vary from site to

site because of varying precursors and atmospheric conditions. It has been widely observed that the intensity (Sihto et al., 2006; Dada et al., 2017) and frequency (Dada et al., 2017; Boy and Kulmala, 2002; Hyvönen et al., 2005) of continental NPF are reduced during periods of high RH, resulting in reduced ultrafine particle number concentrations during these periods (Weber et al., 1997). For example, 20 years of observations in the boreal forest at Hyytiälä, Finland, showed that NPF is more likely to happen during periods of low ambient RH (Dada et al., 2017). In urban areas, NPF also favors low RH (Cai et al., 2017; Shen et al., 2011). Despite the low continental NPF event frequency at high RH, NPF has still been observed in the free troposphere in vicinity of clouds, where RH is extremely high (Weber et al., 1999) and in coastal and marine areas where RH is typically greater than 90% (O'Dowd et al., 1998).

The widely observed anti-correlation between NPF and RH in the field experiments can be attributed to the indirect influence of water. For example, high RH often corresponds to greater cloud cover, which can lead to lower ground-level concentrations of photo-oxidized precursors such as H₂SO₄ and HOMs as well as an increased condensation sink that leads to scavenging of precursors and clusters (Hamed et al., 2011). On the other hand, water vapor may also directly influence NPF by regulating the formation of gas phase precursors or by participating in cluster formation. For example, chamber and model experiments on the binary sulfuric acid-water system have demonstrated positive relationships between particle formation rate and RH (Duplissy et al., 2016; Merikanto et al., 2016). While in the ternary (H₂SO₄/MSA-H₂O-Amine/NH₃) system, H₂O was reported to have either positive (Chen et al., 2015) or negative (Napari et al., 2002) effects on NPF. Some studies have hypothesized that high water content might suppress the formation of NPF-related organics from the oxidation of biogenic precursors (Hyvonen et al., 2005; Boy and Kulmala, 2002). However, no direct evidence of this has been provided.

Although sulfuric acid has been recognized as the most important precursor of new particle formation, it alone can't explain the rapid formation and growth rates observed in the field (Kuang et al., 2008). Organic compounds, ammonia, amines, and water are also likely involved (Zhang et al., 2012; Chen et al., 2012; Yu et al., 2012). Organics have been shown to be very important for cluster formation and stabilization in theoretical studies (Ortega et al., 2016; Donahue et al., 2013), laboratory experiments (Tröstl et al., 2016; Schobesberger et al., 2013) and field measurements (Bianchi et al., 2016; Hoffmann et al., 2001; Metzger et al., 2010). Organics can either form clusters with sulfuric acid or purely with themselves (Zhao et al., 2013; Zhao et al., 2009). They can also contribute significantly to the condensational growth of newly formed particles, determining particle growth rates, particle lifetime, and global particle and CCN concentrations (Donahue et al., 2011; Vehkamäki and Riipinen, 2012). The ability of organics to take part in particle formation and condensational growth depends

on their volatility as well as reactivity. HOMs, such as extremely low volatility organic compounds (ELVOCs, saturation mass concentration (C^*) < 3×10^{-4} µg m⁻³) or low volatility organic compounds (LVOCs, 3×10^{-4} < C^* < 0.3 µg m⁻³), are likely contributors to NPF (Donahue et al., 2012; Ehn et al., 2014).

Despite its large contribution to NPF, the direct measurement of HOMs has long been a challenge because of their low atmospheric concentrations, low volatilities, and short lifetimes. Recently, the development of the high resolution time-of-flight chemical ionization mass spectrometer (HRToF-CIMS) overcame this barrier and made the measurement and identification of HOMs feasible (Junninen et al., 2010; Jokinen et al., 2012). HOMs from both monoterpene and aromatic oxidation showed high O/C ratios of >0.7 - 0.8, and were present as monomers, dimers and even higher order clusters (Molteni et al., 2018; Ehn et al., 2012). These high O/C ratios could not be explained by any of the formerly known oxidization pathways unless the autoxidation of RO₂ was taken into consideration (Crounse et al., 2013; Barsanti et al., 2017). The autoxidation of RO₂ includes intramolecular hydrogen shifts and O₂ additions. Several repetitions of the autoxidation cycle lead to a rapid increase in oxygen content as well as a decrease in saturation vapor pressure. Autoxidation was widely observed in condensed phase reactions, however, it was not considered in the gas phase previously due tof the perception of a high barrier for the intramolecular hydrogen shift. This was confirmed by the fact that at higher temperatures, more HOMs are formed than at low temperatures (Frege et al., 2018). Modeling studies now show that intramolecular hydrogen shifts are fast enough to compete with bimolecular sink reactions (Kurten et al., 2015).

Since most laboratory experiments related to the formation of HOMs have been conducted under conditions of constant RH, usually low or medium RH of less than 60% (Ehn et al., 2012; Zhang et al., 2015), it was still unknown whether and how water vapor might impact HOM formation. High RH conditions are difficult to achieve in chamber experiments without significantly changing temperature and pressure. In addition, HOM detection by the current commercially available CIMS inlet based on the design of Eisele and Tanner is subject to water cluster influence at high RH (Kürten et al., 2016).

In this research, three different endocyclic monoterpenes, α -pinene, limonene and Δ^3 -carene were reacted with ozone, with and without hydroxyl radical (OH) scavengers, in a reaction flow tube to generate secondary organic aerosol (SOA). RH influences on HOM formation and organic-driven NPF were studied under a range of RH from ~3% to ~92%. Generated closed-shell HOMs and RO₂ were measured using a home-built CIMS inlet coupled to a HRToF mass spectrometer (LTOF mass analyzer, Tofwerk AG). The CIMS inlet effectively reduced water clustering onto ions sampled into vacuum, thus removing sample artifacts caused by high water vapor levels. Water vapor influence on the formation of RO₂, HOM

monomers and HOM dimers were studied. The volatility of O₃- and OH-derived closed-shell HOMs were estimated with a group contribution-based model (SIMPOL) and a recently developed statistical model to study the potential contribution of O₃ and OH initiated chemistry on NPF.

2 Methods

91

92

93

94

95

96

97

98

99

100

101

102

103

104

105

106

107

108

109

110

111

112

113

114

115

116

117

118

119

2.1 Flow tube reactor

The experiments were performed in a laminar flow tube reactor consisting of a 150 cm long Pyrex glass cylinder with a volume of 8.5 dm³ (Figure 1). The flow tube was located in a temperature controlled room ($T = 293 \pm 2$ °C) and was covered so that all experiments were performed under dark conditions. For these experiments, dry "zero air" was generated with a zero air generator (model 747-30, Aadco Instruments), with NOx and SO₂ concentrations each specified to be less than 0.5 ppbv. The monoterpenes were injected into the flow tube using a syringe pump (model NE-300, New Era Pump Systems, Inc.) evaporated into a 2.5 LPM flow of dry zero air. O₃ was generated by passing 0.5 LPM dry zero air (79% N₂, 21% O₂) over a Hg UV lamp (model 90-0004-04, UVP, LLC) and then diluted with 6.5 LPM of humidity-controlled zero air. A temperature-controlled bubbler filled with deionized water was used to generate humid air, and the prescribed RH was achieved by controlling the temperature of the bubbler. An ozone analyzer, described below, sampled at 1 LPM, resulting in a total flow rate of 8.5 LPM and a corresponding reaction time of ~60 s for each experiment. Gas inlets to the flow tube were made from 0.64 cm outside diameter Teflon tubes that were capped and drilled with ~1 mm holes to distribute sample air uniformly into the flow tube, as described and modeled in Ball et al., (1999). The uniform distributions of O₃ and H₂O in the flow tube were confirmed by measuring $[O_3]$ and RH at the different locations prior to the experiments. In every experiment, RH was adjusted to be constant for at least 30 min for each of the four RH steps (3-5%, 30-38%, 58-65%, 85-92%). In order to achieve the highest relative humidity stage, the temperature of the humid flow was saturated at 26 °C before being mixed with room temperature air from the monoterpene source. This resulted in a slightly higher temperature at the inlet of the flow tube, which could contribute to lower nucleation rates (Burkholder et al., 2007). Nevertheless, over the range of the first three humidity stages, up to 65% RH, the gas temperature was constant before, during, and after reaction. At the beginning of the experiments, the inner wall of the reactor was washed with ultra-pure water. All of the flow rates were calibrated before and during the experiments.

2.2 Instrumentation

2.2.1 Transverse Ionization – Chemical Ionization Mass Spectrometer

A self-designed and home-built chemical ionization inlet, called Transverse Ionization (TI) inlet (Figure 2 and Figure S1), was used in front of the LTOF mass analyzer. The TI design is similar to those of the Ambient-pressure Proton transfer Mass

Spectrometer (AmPMS) (Hanson et al., 2011) and the cluster-CIMS (Zhao et al., 2010). In the TI inlet, a 4 - 10 LPM flow of sample air is passed across the inlet orifice of the mass spectrometer, where it encounters an orthogonal, 1 LPM reagent ion gas flow consisting N_2 containing ionized nitrate ions (NO_3) as well as potential cluster ions (HNO_3)_n NO_3 with n = 1-3. For the current study, the sample flow to the inlet was set to 4.5 LPM. Chemical ionization occurs at atmospheric pressure and temperature. The reagent gas is generated by passing 3 ccm of N_2 over a small vial containing nitric acid, which is then ionized by a 370 MBq Po^{210} radioactive source (model P-2021, NRD, LLC). An additional flow of N_2 can be added to the reagent gas to change the reagent ion concentration, and the assembly can be adjusted to vary ion-molecule reaction time. The latter can be controlled by adjusting the sample and reagent gas flow rates or by applying different voltages to the ionization source and the main inlet block. To minimize the diffusion loss in sample lines, the inlet of the TI source was connected to the flow tube outlet by a short (~10 cm) piece of electro-polished stainless steel tubing. Compared to the widely used commercial nitrate inlet patterned after the design by Eisele and Tanner (1993) and marketed by Aerodyne, Inc., no additional sheath flow is required thus any impurities potentially introduced by the sheath flow are eliminated. Some flow disturbance may occur where the sample flow encounters the transverse reagent flow, which may lead to non-ideal behavior. However, even at the maximum total flow of 11 LPM, the reynolds number in this region is ~500 thus turbulence is not expected to be significant.

Another unique aspect of the TI design is the use of an N_2 curtain gas in front of the inlet orifice to the mass spectrometer to reduce water clustering on reagent and sample ions. Water clusters are expected to form at high RH mainly during the free-jet expansion of the sampled gas on the vacuum side of the orifice plate (Thomson and Iribarne, 1979). The presence of these clusters makes the identification and quantification of both sample and reagent ions challenging (Kulmala et al., 2014; Lee et al., 2014; Kürten et al., 2016; Ehn et al., 2014). Figure 2 shows the details of the TI source that address this issue. Small holes drilled in a radial channel blow N_2 uniformly in front of the orifice plate so that only sampled ions and this clean N_2 gas pass into the vacuum chamber. Since the sampling flow rate of the mass spectrometer is ~ 0.7 LPM when using 0.3 mm orifice, the N_2 curtain flow is set to be 1 LPM to overflow the region surrounding the orifice. By applying voltages to the ion source and the block, the ions can be efficiently guided into the mass spectrometer while neutral molecules such as water vapor are prevented from entering by the N_2 curtain gas.

This TI inlet is suitable to all types of reagent ion chemistry, e.g. NO₃, Γ, and H₃O⁺. Nitrate ion chemistry was used as the reagent ion in these experiments, which is selective to highly oxidized molecules that have at least two hydroperoxy (-OOH) groups or some other H-bond-donating groups (Hyttinen et al., 2015). HOM monomers, HOM dimers and highly oxidized

RO₂ radicals can also be measured using nitrate ion chemistry.

2.2.2 Other measurements

Ozone concentrations were measured with two ozone analyzers (model 106L, 2B Technology) at the inlet and outlet of the flow tube. The sampling flow of each analyzer is 1 LPM. The two ozone analyzers were intercompared prior to the experiments and the difference was within 5 ppbv when [O₃] < 1000 ppbv. A Scanning Mobility Particle Sizer (SMPS), consisting of a Po210 bipolar neutralizer, a nano-Differential Mobility Analyzer (nano-DMA; model 3081, TSI, Inc.), and a condensation particle counter (MCPC; model 1720, Brechtel Manufacturing) were used to measure the number-size distribution of particles, which is later used to deduce the total particle number and mass concentrations (the latter assumes a uniform density for organic particles of 1.2 g cm⁻³). The sampling flow rate of the MCPC was 0.3 LPM and the sheath and excess flows of the nano DMA were set to 3 LPM. The flow tube particle number-size distribution was measured without further drying to get a more accurate measure of the actual particle surface area and volume, which are important for HOM partitioning, and also to prevent particle evaporation during the measurements.

2.3 Experimental conditions

Three monoterpenes were used in our experiments (see Table 1), α -pinene, limonene and Δ^3 -carene. Oxidation by ozone is believed to dominate over other oxidation radicals (i.e., OH or NO₃) in forming SOA under atmospheric conditions (Atkinson and Arey, 2003). Ozonolysis of alkenes generates a substantial amount of OH, leading to products that are produced by a combination of O₃ and OH oxidation. For some experiments, in order to isolate oxidation by O₃, cyclohexane (see Table 1 for mixing ratios) was premixed with the monoterpene and added to the flow tube as an OH scavenger. For other experiments, the combination of OH and O₃ chemistry were investigated to study atmospheric oxidation chemistry more representative of ambient air. The "high concentration" experiments were conducted with similar mixing ratios of monoterpene (~1100ppb) and O₃ (~900ppb). The "low concentration" experiments were conducted to study the particle-free chemical processes with initial concentrations of monoterpenes and O₃ shown in Table 1. Since wall losses should be comparable for different precursors as a function of RH, it was not taken into consideration in our analysis of HOM production.

2.4 HOM volatility predictions

The SIMPOL.1 method (Pankow and Asher, 2008) and the molecular corridor method (Li et al., 2016) were used to predict the saturation mass concentrations (C^*) of some of the detected OH- and O₃-related HOMs. SIMPOL.1 is a group

contribution method and requires information on molecular structure, while the molecular corridor method only requires the molecular formulae. Both methods are semi-empirical and based on volatility data from hundreds or thousands of compounds. The calculated volatilities were then applied to the two-dimensional volatility basis set (2D-VBS) (Donahue et al., 2012) to explore the likelihood that the products participate in the initial stages of nanoparticle growth.

3 Results and discussion

3.1 TI-CIMS performance

When comparing the TI inlet with the commercial nitrate inlet in measuring α -pinene ozonolysis products, both inlets produced identical mass spectra. The sensitivities of both inlets to H_2SO_4 were determined using a home-built H_2SO_4 calibration system (Figure S2) based on the design of Kürten et al. (2012). Figure 3 summarizes the results of these calibrations. The position of the ion source assembly relative to the inlet orifice is critical for determining the sensitivity of the TI inlet. When the ion source is placed 0.5 cm upstream along the sample flow axis and 5 cm away from the inlet orifice along the reagent ion flow axis (configuration shown in Figure 2), the instrument is at its most sensitive. The calibration factors, defined as $C = [H_2SO_4]/([HSO_4^-]/[NO_3^-])$ (Eisele and Tanner, 1993), for the TI in this position and the commercial inlet were 3.25×10^{10} molecules cm⁻³ and 1.41×10^{10} molecules cm⁻³, respectively. The lower calibration factor for the TI inlet is attributed to the shorter reaction time (~80 ms) compared to the commercial inlet (~200 ms). We note that the reaction time of the TI inlet can be further increased by positioning the ion source assembly further upstream relative to the inlet orifice, which would require a slight modification of the current design. The total ion counts (TIC) of the TI inlet are more than 5 times higher than the commercial inlet, which we attribute to the more direct path of ions through the ion source as well as the use of a Po^{210} radioactive source as compared to the soft X-ray in the commercial nitrate inlet. The limit of detection (LOD) for sulfuric acid, which is defined as three times the standard deviation of the background (Jokinen et al., 2012), is 9.3×10^4 molecules cm⁻³ and 1.26×10^5 molecules cm⁻³ for the TI and commercial inlets, respectively.

After applying the N_2 curtain gas flow, the TIC recorded by the TI-CIMS decreased significantly. This was compensated for by increasing the ion source and reaction chamber voltages that direct ions to the orifice (Figure S3). When RH \approx 90%, the reagent ion mass spectrum was dominated by water clusters $(H_2O)_m(HNO_3)_nNO_3^-$ (m = 0-30, n = 0-2) if no N_2 curtain flow was applied (Figure 4a). The reagent ions NO_3^- , $HNO_3NO_3^-$ and $(HNO_3)_2NO_3^-$ decreased as RH increased, with $[(HNO_3)_2NO_3^-]$ and $[HNO_3NO_3^-]$ decreasing much faster than $[NO_3^-]$. In contrast, after 1 LPM N_2 curtain flow was applied to the inlet, most of the water clusters were removed (Figure 4b). The reagent ions, sample ions and TIC remained stable as RH

increased, which resulted in a reliable measurement of HOM concentrations as a function of RH. The result that the N_2 curtain flow eliminated water clustering to a large extent confirms that most of the water clusters in the spectrum were produced during the free-jet expansion into vacuum instead of formed in the ion-molecular reagent region.

3.2 Identification of HOM spectrum

Figure 5 shows the average mass spectra of the HOM dimers and Figure S4 shows the average mass spectra of the HOM monomers and RO₂ radicals for each of the six particle generation experiments. More than 400 peaks were identified in each spectrum, the majority of which were clusters with NO₃ or HNO₃NO₃. [H₂SO₄], which arises from the oxidation of trace amounts of SO₂ in the aero air, was ~10⁵ molecules cm⁻³ and was always less than 3% of the most abundant C₁₀ products, suggesting that sulfuric acid plays a negligible role in nucleation and cluster growth in our experiments. After subtracting the reagent ions (NO₃ or HNO₃NO₃), molecular formulae for organics with an odd number of H atoms were assigned to radicals, which are generally difficult to detect experimentally (Rissanen et al., 2015), and formulae with an even number of H atoms were assigned to closed-shell molecules. Most of the HOM products from the three endocyclic monoterpenes were very similar, while the relative abundance of different HOMs was quite different, indicating similar reaction pathways but different branching ratios in the reaction mechanisms. The main products were C₅₋₁₀H₆₋₁₆O₃₋₁₀ for closed shell monomers and RO₂ and C₁₅₋₂₀H₂₂₋₃₄O₆₋₁₈ for closed shell dimers. Among these, C₁₀ and C₂₀ compounds were the most abundant. C₅₋₉ products could be formed from O₃ attack on the less reactive exocyclic carbon double bond or the decomposition of intermediate radicals. Some fragments were found to be unique for specific monoterpene precursors. For instance, C₃H₆O₇ (m/z 240) was much more abundant in α-pinene oxidation than from other two precursors, which might be a tri-carboxylic acid (Ehn et al., 2012).

Comparing total HOM abundance for the three monoterpene oxidation reactions, limonene created the most, followed by α -pinene and then Δ^3 -carene. This is in qualitative agreement with prior studies (Jokinen et al., 2014; Ehn et al., 2014). The total dimer signal intensity was 15-30% of monomers for all three monoterpenes. Experiments with an OH scavenger generated fewer HOMs than those without OH scavengers.

As observed in previous studies, $C_{10}H_{15}O_{6,8,10,12}$ and $C_{10}H_{17}O_{5,7,9,11}$ comprised the O_3 - and OH-related RO_2 , respectively (Jokinen et al., 2014). $C_{10}H_{14}O_{5,7,9,11}$ comprised the O_3 -related closed shell monomers, while $C_{10}H_{16}O_{6,8,10,12}$ and $C_{10}H_{18}O_{6,7}$ comprised the OH-related closed shell monomers (Ehn et al., 2014; Berndt et al., 2016). When comparing the average spectra with and without OH scavenger, no obvious differences were seen for OH-related RO_2 or monomers (Figure S4). In

contrast, for dimers we found that $C_{20}H_{32}O_{6-13}$ were more abundant in experiments without OH scavenger (Figure 5). The formation of these dimers can be explained by the reaction of one OH-related RO_2 with one O_3 -derived RO_2 (see Section 3.5), and can therefore be considered as markers for combined OH and O_3 chemistry. As HOM dimers are generally less volatile than monomers with identical O/C ratio, rapid production of dimers is believed to play a more important role in initial particle formation and growth (Zhang et al., 2015).

3.3 RH influence on HOM generation

Figure 6 shows a time series of experimental parameters, particle size distribution, and key ions from the limonene ozonolysis experiment with OH scavenger (EXP. 2 in Table 1). The O₃ inlet and outlet concentrations were approximately constant with increasing RH (Figure 6a), indicating that RH did not significantly change O₃ levels in the flow tube. This also shows that the reactivity of the limonene with ozone does not change with RH. The number concentration of the generated particles decreased from 4.9×10^6 cm⁻³ to 2.7×10^6 cm⁻³ with increasing RH, while the peak of the number-size distribution increased slightly, due in part to water absorption. When RH was above 80%, both the integrated number and mass concentrations, which were calculated from the number-size distributions, decreased (Figure 6b).

Despite the change in particle number and mass concentrations with RH, the concentration of all the main HOMs, including RO₂, monomers and dimers, did not change for both OH- and O₃-derived products (Figure 6c). In fact, the only signals in the mass spectra that changed with RH corresponded to an increases associated with water clusters. The variations in HOM concentrations can be explained by the competition between production and condensational losses. As almost all of the detected HOMs are ELVOCs or LVOCs (see Section 3.6), they are not likely to partition back to the gas phase after they encounter a surface. The condensation sink (CS) and wall loss rate for a compound with diffusion coefficient of 8.5×10^{-6} m² s⁻¹ (e.g., sulfuric acid) were estimated using established methods (Kürten et al., 2014; Crump and Seinfeld, 1981; Kulmala et al., 2001). The calculated CS varied between 0.1-3.5 s⁻¹ in different SOA generation experiments, much larger than the wall loss rate (< 0.01 s⁻¹). There was about 5-30% variation in CS in each SOA generation experiment from RH = 3% to 92%. This amount of variation in CS does not seem to have a noticeable influence on the final concentration of HOMs. To further test the hypothesis that variations in condensation sink do not impact final HOM concentrations, particle free experiments were performed and, again, detected HOM concentrations did not change with RH (Figure 7).

3.4 RH influence on SOA generation

Figure 8 shows the integrated SOA particle number and mass concentrations over the observed diameter range of 10 - 100

concentrations and 470-1025 μ g m⁻³ for mass concentrations) were ~3-12 times greater than for \triangle ³-carene (0.3-2.0 × 10⁶ cm⁻³ for number concentrations and 56-86 μ g m⁻³ for mass concentrations) and α -pinene (0.4-2.2 \times 10⁶ cm⁻³ for number concentrations and 61-130 µg m⁻³ for mass concentrations). This is because the theoretical ozone reactivity of limonene is 3~5 times higher than the latter two and molar yield from limonene ozonolysis is also the highest. Peaks in the particle number-size distributions were between 40 and 70 nm (Figure S5). In most of the experiments, generated SOA mass concentrations increased or decreased slightly when RH increased from ~0% to ~60% and decreased as RH further increased to ~90%. The variability in particle mass concentration as a function of RH for different experiments can be attributed to combined effects of gas phase reactions, condensed phase reactions, physical uptake of water, as well as the re-evaporation of semi-volatile compounds from the wall. We cannot accurately quantify these effects. As a result, although the measured SOA mass concentration remained relatively constant, we cannot draw conclusions from this observation. In contrast, while particle number concentrations may also be affected by the factors mentioned above, they decreased by a factor of 2~3 with increasing RH. A number of studies have demonstrated different water and OH influences on the ozonolysis products of exocyclic and endocyclic organic compounds. They have reported either suppressing (Bonn et al., 2002; Bonn and Moorgat, 2002) or promoting (Jonsson et al., 2006; Jonsson et al., 2008) effects of water vapor on the particle formation processes during ozonolysis of monoterpenes by measuring the number-size distributions of generated SOA particles with SMPS. The discrepancies between different results could be attributed to the different experiment setups, e.g., monoterpene and O₃ concentration, temperature, RH range, OH scavengers, reaction time, and so on. Specifically, our results are in good agreement with those of Bonn et al., who studied SOA generation from the ozonolysis of endocyclic monoterpenes (Bonn et al., 2002). In that study, SOA number concentrations decreased by a factor of 1.1~2.5 as RH increased, while the variation in volume concentrations was negligible (within ±10%). They concluded that water's influence on non-volatile products, which are responsible for the initial steps of nucleation, was much larger than its influence for semi-volatile compounds which mainly determined the final volume concentrations of particles. Thus, it was highly suspected that water influenced new particle formation through influencing the generation of NPF precursors. However, our measurements indicate that at least the formation of the detected HOMs is independent of water vapor concentrations. There may be other species that are crucial to the initial steps of NPF and are affected by water vapor but are not detected by nitrate CIMS (see section 3.5). Another possible explanation is that a fraction of HOMs cluster with water at high RH in such a way that they may no longer be able to participate in further cluster formation, thereby suppressing NPF. If the CIMS measurement only detected the declustered molecule, then such a mechanism may still be consistent with our observations.

nm. The generated SOA particle number and mass concentrations for limonene (2.2-6.0 × 10⁶ cm⁻³ for number

269

270

271

272

273

274

275

276

277

278

279

280

281

282

283

284

285

286

287

288

289

290

291

292

293

294

295

296

297

301

302

303

304

305

306

307

308

309

310

311

312

313

314

315

316

317

318

319

320

321

3.5 Possible formation pathways of water-relevant C₁₀ and C₂₀ HOMs

Although the oxidation of BVOCs has been widely studied, it has mostly been constrained to the early stages (first and second generation intermediates) and many uncertainties still exist (Johnson and Marston, 2008; Isaacman-VanWertz et al., 2018; Atkinson and Arey, 2003). The first step of ozonolysis for the three BVOCs (α -pinene, Δ ³-carene and limonene) is ozone attack on the endocyclic carbon double bond to form a primary ozonide. Figure 9 shows the O₃-initiated oxidation pathways of α-pinene that may be related to the detected C₁₀ and C₂₀ HOMs for representative isomers. The primary ozonide rapidly transforms to two excited Criegee intermediates (eCIs), one of which (branching ratio= 0.4) (Kamens et al., 1999) is shown in Figure 9. The reaction pathways of the eCI are complex, the most important two under ambient and most chamber conditions are the sCI channel (reaction I) and the hydroperoxide channel (reaction II) (Bonn et al., 2002). The sCI either reacts with aldehydes to form a secondary ozonide (when the aldehyde is C₁₀, then the formed SOZ is C₂₀ and is marked as sCI-C₁₀) or with water or other acidic compounds such as alcohols and carboxylic acids to form hydroxy-hydroperoxide, which then decomposes to carboxylic acids or aldehydes. For α-pinene, the main decomposition product is pinonic acid. In the hydroperoxide channel (reaction II), the formed hydroperoxide quickly decomposes to a first generation alkyl radical (R) and OH (Johnson and Marston, 2008). R reacts with O2 immediately to form the first generation RO2, which can undergo numerous reactions, including reaction with HO2, R'O2 and autoxidation. The reaction with HO2 mainly forms hydroperoxides, with a small fraction forming hydroxyl or carbonyl-containing compounds. When reacted with another R'O₂, either ROOR' or an alkoxy radical (RO) or a carbonyl and a hydroxyl are formed. The RO can undergo isomerization, or form a carbonyl and HO2, for which the branching ratios are extremely difficult to evaluate. RO can also undergo decomposition, which is one of the pathways to form $C_5 \sim C_9$. The autoxidation process is key to HOM formation. Each autoxidation step adds two O atoms to the molecule and thus increases the oxidation state very rapidly. The competition between autoxidation processes and bimolecular reactions (RO2 reactions with R'O2 or HO2) determines the ultimate oxidation state of the products (Barsanti et al., 2017; Crounse et al., 2013; Rissanen et al., 2015).

322

323

324

325

326

327

328

OH can be generated in the ozonolysis of alkenes and the yield is near unity (Atkinson, 1997). The reaction of OH with α -pinene directly forms first generation R and then RO₂; one possible structure for this RO₂ (branching ratio = 0.44), formed from OH addition to the double bond (Berndt et al., 2016), is shown in Figure 9. However, the formed RO₂ (C₁₀H₁₇O_{2m+1}) are not the same RO₂ as those formed through ozonolysis (C₁₀H₁₅O_{2n+2}) (McVay et al., 2016). Accordingly, the structure and composition of C₁₀ and C₂₀ HOMs formed from OH or O₃ chemistry are different, and so too are their potential impacts on NPF. The combined OH- and O₃-derived dimers (C₁₀H₃₂O_{2(m+n)+3}), formed by collision of an OH-derived RO₂ with an

O₃-derived RO₂, were only observed in ozonolysis experiments without OH scavenger.

The RO₂ autoxidation pathway explains most of the observed C_{10} and C_{20} compounds in the mass spectra. One exception to this is that $C_{10}H_{18}O_{2m+1}$, $C_{10}H_{18}O_{2m}$ and $C_{20}H_{34}O_{2(m+m')}$ were not observed in the spectrum whereas in experiments performed by Berndt et al., in which OH oxidation for α -pinene was studied, $C_{10}H_{18}O_{2m}$ and $C_{20}H_{34}O_{2(m+m')}$ dominated the mass spectrum (Berndt et al., 2016). This could be explained by a lower OH/O₃ ratio in our experiments, since unlike Berndt et al. we did not provide an extra source of OH to the flow tube. Also, Berndt and coauthors reported lower sensitivity of nitrate reagent ions to OH-related RO2 compared to other reagent ions such as acetate.

Despite this close agreement achieved by the RO₂ autoxidation mechanism and the observed mass spectra in our study, prior studies suggest that other potential pathways cannot be excluded. An accretion product involving sCI is one possibility (Barsanti et al., 2017). It is possible that sCI reacts with long-chain carboxylic acids or carbonyls, such as those with 10 carbon atoms, forming in this instance anhydrides (sCI-C₁₀, reaction IV) or secondary ozonides (sCI-C₁₀, reaction V) with vapor pressures lower than 10⁻¹⁵ torr (Kamens et al., 1999; Tobias and Ziemann, 2001; Bonn et al., 2002). The formation of anhydride is more likely in condensed phase, whereas there is also a possibility it can also happen in gas phase (Kamens et al., 1999). However, it is unknown whether these sCI-C₁₀ can be detected using nitrate-CIMS as they may lack hydrogen bond donor moieties. The semi-volatile pinonic acid can also form HOMs after further oxidation by OH (Ehn et al., 2014), provided that excess α-pinene is not present to compete with pinonic acid for the generated OH.

Water vapor's influence on HOM formation can be direct or indirect. For monoterpene oxidation, the direct participation of water vapor is to react with sCI, favoring the formation of the hydroperoxide and its decomposition products (reaction III) over the secondary ozonides (sCI-C₁₀, reaction IV) or possible anhydrides (sCI-C₁₀, reaction V). Since the formation of sCI-C₁₀ is more likely to contribute to NPF than the products from sCI and water vapor (Kamens et al., 1999; Tobias et al., 2000), a decrease in low volatility sCI-C₁₀ with high RH could explain the decreasing SOA number concentrations in our experiment. It has been shown previously that OH yields from the reactions of O₃ with a series of monoterpenes were not affected by the presence of water vapor (Atkinson et al., 1992; Aschmann et al., 2002), which implies that the hydroperoxide channel (reaction II) are similarly unaffected by water. Since the detected HOMs in our experiments were RH-independent, we conclude that all the detected HOMs were formed from hydroperoxide channel (reaction II) and not via the sCI channel (reaction I). Similarly, the detected HOMs were not likely to form through the hydration reaction (Equation 1) (Ehn et al., 2012), which is supposed to increase with increasing RH.

$$R - CHO + H2O \rightarrow R - CH(OH)2 (Equation 1)$$

The indirect water effect on HOM formation includes the water influence on HO₂ fate. As water promotes HO₂ self-reaction (Equation 2), reaction of HO₂ with RO₂ should decrease and the related HOM monomers should likewise decrease with increasing RH. However, as the formation of both HOM monomers and dimers was not affected by H₂O, it was likely that water does not significantly increase HO₂ self-reaction or that HO₂ chemistry was not important in our experiments.

$$2HO_2 \xrightarrow{M, H_2O} H_2O_2 + O_2$$
 (Equation 2)

3.6 Volatility predictions

360

361

362

363

364

366

367

368

369

370

371

372

373

374

375

376

377

378

379

380

381

382

383

385

386

387

The volatility of the gas phase products is one of the most important properties that determines whether a compound contributes to the formation, initial growth or further growth of SOA particles (Donahue et al., 2012; Kroll et al., 2011). As the products with identical elemental composition can be formed from different bimolecular reactions of the intermediate RO2, it is difficult to predict their exact structures. For the current study, the number of different structural and functional groups (e.g., aromatic rings, aldehydes, ketones, hydroxyls, peroxides, hydro-peroxides) was estimated and used to derive saturation vapor pressure using SIMPOL.1 (Table S1). To simplify the calculation, the functional groups used here were directly predicted from the proposed formation pathways in Figure 10 and did not include intramolecular isomerization, although that may be important in some situations. For example, one of the ROOH can be replaced with an endo-peroxide via ring closure of unsaturated RO₂ (Berndt et al., 2016). It has to be noted that the group contribution methods very likely underestimate the volatility of HOM product from α-pinene autoxidation products due to ignoring intramolecular H-bonding (Kurtén et al., 2016). There may be large uncertainties in SIMPOL method as well as in our functional group estimation process. As a comparison, the Molecular Corridor method (Li et al., 2016), which does not require information on functional groups, was used to estimate the saturation vapor pressure as well. The average carbon oxidation state $(\overline{OS}c)$ was calculated with Equation 3, in replacement of the commonly used formula $(\overline{OS_C} = 20: C - H: C)$, as the second oxygen atom in (hydro) peroxide group does not increase the carbon oxidation state. In equation 3, n_0 , n_C , and n_H are the oxygen, carbon, and hydrogen numbers in the molecule; $n_{(hydro)peroxide}$ is the number of (hydro) peroxide groups in the molecule.

$$\overline{OS}_C = \frac{2n_O - n_{(hydro)peroxide} - n_H}{n_C}$$
 (Equation 3)

Figure 10 shows the predicted saturation mass concentrations (C*) of the main C_{10} and C_{20} closed shell products. The difference of C* predicted from the two methods was ~1-4 orders of magnitudes. Despite these differences, most of the C_{20} HOMs can be classified as ELVOCs, while C_{10} products were mostly LVOCs. Typically, t for those compounds with

identical $\overline{OS}c$, such as $C_{20}H_{30}O_{10}$ (O₃-derived dimer, $log_{10}(C^*)$ =-2.74), $C_{20}H_{32}O_{11}$ (OH and O₃ combined dimer, $log_{10}(C^*)$ =-5.11), $C_{20}H_{34}O_{12}$ (OH-derived dimer, $log_{10}(C^*)$ =-7.41), OH-derived HOMs have lower volatilities than O₃-derived HOMs due to a greater number of (hydro) peroxide groups.

391

392

393

394

395

396

397

398

399

400

401

402

403

404

405

406

407

408

409

388

389

390

4 Conclusions

The RH influence on HOM formation and NPF during monoterpene oxidation was explored in this study. HOMs were detected with a TI-CIMS, using nitrate as reagent ions; C₁₀ and C₂₀ dominated the spectra. There are mainly three potential paths for water vapor influence on the formation of C₁₀ and C₂₀ HOMs. One is water reacting with sCI (Equation 1), thereby influencing the branching ratio between formation of more volatile compounds decomposed from hydroxyl hydroperoxide, such as pinonic acid, and accretion products with sCI such as secondary ozonide (sCI-C₁₀) and anhydride (sCI-C₁₀). The second hypothesized water influence is on the HOMs formed from hydration reactions (Equation 2). The third is that water increases the rate of self-reaction of HO₂ (Equation 3), thus indirectly impacts the loss pathways of RO₂. Our experimental results, both with high particle loading and particle-free conditions, demonstrated that neither the detected HOM species nor their signal abundance changed significantly with RH. This indicates that the detected HOMs, which can mostly be explained by RO₂ autoxidation, must be formed from water-independent pathways rather than by those reactions mentioned above. One implication of this result is that HO2 self-reaction was not significantly promoted by water or that the RO2 reaction with HO₂ was not be significant in our system, but instead that RO₂ reacts with another peroxy radical, R'O₂, to generate both closed shell monomers and dimers. Another implication is that the sCI pathway is not responsible for the generation of the detected HOMs while the role of sCI-related HOMs (SOZ or anhydride) formation by accretion with long chain products, which may not be detected with nitrate CIMS, may be important in causing the decrease in SOA number concentrations with increased RH. Another possible explanation for the decreasing SOA number concentration is that water may cluster with HOMs and suppress NPF.

410

411

412

413

414

415

416

The detected HOMs, which could mostly be explained by autoxidation of RO_2 followed by reactions with $R'O_2$ or HO_2 , were distinguished as OH-related, O_3 -related RO_2 , closed shell HOM monomers, and HOM dimers. The volatility of the identified products were estimated with the SIMPOL.1 group contribution method and with the molecular corridor technique. That analysis confirmed that C_{20} closed shell products have significantly lower volatility compared to C_{10} products and are thus more likely to contribute to NPF. For the HOM products with identical $\overline{OS}c$, OH-derived HOMs have lower volatilities than O_3 -derived HOMs due to a greater number of (hydro) peroxide groups. As a result, OH chemistry is suspected to be more

likely to lead to NPF than O₃ chemistry, given the same level of oxidants and VOCs precursors.

418

419

Acknowledgements

- 420 This research was supported by the US Department of Energy's Atmospheric System Research program under grant no
- 421 DE-SC0019000, the US National Science Foundation under grant no. AGS-1762098, and by the National Key R&D
- 422 Program of China under grant no. 2017YFC0209503. XL thanks the financial support from the State Scholarship Fund
- 423 managed by Chinese Scholarship Council (CSC). We thank Hayley Glicker, Deanna Caroline Myers, Michael Lawler, and
- 424 Danielle Draper for their kind help.

425

426

References

- 427 Andreae, M. O., Afchine, A., Albrecht, R., Holanda, B. A., Artaxo, P., Barbosa, H. M., Borrmann, S., Cecchini, M. A., Costa,
- 428 A., and Dollner, M.: Aerosol characteristics and particle production in the upper troposphere over the Amazon Basin, Atmos
- 429 Chem Phys, 18, 921-961, 2018.
- 430 Aschmann, S. M., Arey, J., and Atkinson, R.: OH radical formation from the gas-phase reactions of O-3 with a series of
- 431 terpenes, Atmos Environ, 36, 4347-4355, 10.1016/s1352-2310(02)00355-2, 2002.
- 432 Atkinson, R., Aschmann, S. M., Arey, J., and Shorees, B.: Formation of OH radicals in the gas phase reactions of O3 with a
- series of terpenes, Journal of Geophysical Research: Atmospheres, 97, 6065-6073, 1992.
- 434 Atkinson, R.: Gas-phase tropospheric chemistry of volatile organic compounds: 1. Alkanes and alkenes, Journal of Physical
- 435 and Chemical Reference Data, 26, 215-290, 1997.
- 436 Atkinson, R., and Arey, J.: Gas-phase tropospheric chemistry of biogenic volatile organic compounds: a review, Atmos
- 437 Environ, 37, 197-219, 2003.
- 438 Ball, S. M., Hanson, D. R., Eisele, F. L., and McMurry, P. H.: Laboratory studies of particle nucleation: Initial results for
- 439 H2SO4, H2O, and NH3 vapors, J Geophys Res-Atmos, 104, 23709-23718, 10.1029/1999jd900411, 1999.
- 440 Barsanti, K. C., Kroll, J. H., and Thornton, J. A.: Formation of Low-Volatility Organic Compounds in the Atmosphere:
- Recent Advancements and Insights, Journal of Physical Chemistry Letters, 8, 1503-1511, 10.1021/acs.jpclett.7b02969, 2017.
- 442 Berndt, T., Richters, S., Jokinen, T., Hyttinen, N., Kurtén, T., Otkjær, R. V., Kjaergaard, H. G., Stratmann, F., Herrmann, H.,
- and Sipilä, M.: Hydroxyl radical-induced formation of highly oxidized organic compounds, Nature communications, 7,
- 444 13677, 2016.
- 445 Bianchi, F., Tröstl, J., Junninen, H., Frege, C., Henne, S., Hoyle, C. R., Molteni, U., Herrmann, E., Adamov, A., and
- Bukowiecki, N.: New particle formation in the free troposphere: A question of chemistry and timing, Science, aad5456,
- 447 2016.
- Bonn, B., and Moorgat, G.: New particle formation during a-and b-pinene oxidation by O 3, OH and NO 3, and the influence
- of water vapour: particle size distribution studies, Atmos Chem Phys, 2, 183-196, 2002.
- Bonn, B., Schuster, G., and Moortgat, G. K.: Influence of water vapor on the process of new particle formation during
- monoterpene ozonolysis, The Journal of Physical Chemistry A, 106, 2869-2881, 2002.
- Boy, M., and Kulmala, M.: Nucleation events in the continental boundary layer: Influence of physical and meteorological
- 453 parameters, Atmos Chem Phys, 2, 1-16, 2002.

- 454 Burkholder, J. B., Baynard, T., Ravishankara, A. R., and Lovejoy, E. R.: Particle nucleation following the O-3 and OH
- 455 initiated oxidation of alpha-pinene and beta-pinene between 278 and 320 K, J Geophys Res-Atmos, 112,
- 456 10.1029/2006jd007783, 2007.
- Cai, R., Yang, D., Fu, Y., Wang, X., Li, X., Ma, Y., Hao, J., Zheng, J., and Jiang, J.: Aerosol surface area concentration: a
- 458 governing factor in new particle formation in Beijing, Atmos Chem Phys, 17, 12327, 2017.
- 459 Chen, H., Ezell, M. J., Arquero, K. D., Varner, M. E., Dawson, M. L., Gerber, R. B., and Finlayson-Pitts, B. J.: New particle
- 460 formation and growth from methanesulfonic acid, trimethylamine and water, Physical Chemistry Chemical Physics, 17,
- 461 13699-13709, 2015.
- 462 Chen, M., Titcombe, M., Jiang, J., Jen, C., Kuang, C., Fischer, M. L., Eisele, F. L., Siepmann, J. I., Hanson, D. R., and Zhao,
- 463 J.: Acid-base chemical reaction model for nucleation rates in the polluted atmospheric boundary layer, Proceedings of the
- 464 National Academy of Sciences, 109, 18713-18718, 2012.
- 465 Crounse, J. D., Nielsen, L. B., Jørgensen, S., Kjaergaard, H. G., and Wennberg, P. O.: Autoxidation of organic compounds in
- the atmosphere, The Journal of Physical Chemistry Letters, 4, 3513-3520, 2013.
- 467 Crump, J. G., and Seinfeld, J. H.: TURBULENT DEPOSITION AND GRAVITATIONAL SEDIMENTATION OF AN
- 468 AEROSOL IN A VESSEL OF ARBITRARY SHAPE, J Aerosol Sci, 12, 405-415, 10.1016/0021-8502(81)90036-7, 1981.
- Dada, L., Paasonen, P., Nieminen, T., Buenrostro Mazon, S., Kontkanen, J., Peräkylä, O., Lehtipalo, K., Hussein, T., Petäjä,
- 470 T., and Kerminen, V.-M.: Long-term analysis of clear-sky new particle formation events and nonevents in Hyytiälä, Atmos
- 471 Chem Phys, 17, 6227-6241, 2017.
- Donahue, N. M., Trump, E. R., Pierce, J. R., and Riipinen, I.: Theoretical constraints on pure vapor-pressure driven
- condensation of organics to ultrafine particles, Geophys Res Lett, 38, 10.1029/2011gl048115, 2011.
- Donahue, N. M., Kroll, J., Pandis, S. N., and Robinson, A. L.: A two-dimensional volatility basis set-Part 2: Diagnostics of
- organic-aerosol evolution, Atmos Chem Phys, 12, 615-634, 2012.
- Donahue, N. M., Ortega, I. K., Chuang, W., Riipinen, I., Riccobono, F., Schobesberger, S., Dommen, J., Baltensperger, U.,
- 477 Kulmala, M., Worsnop, D. R., and Vehkamaki, H.: How do organic vapors contribute to new-particle formation?, Faraday
- 478 discussions, 165, 91-104, 10.1039/c3fd00046j, 2013.
- Dunne, E. M., Gordon, H., Kürten, A., Almeida, J., Duplissy, J., Williamson, C., Ortega, I. K., Pringle, K. J., Adamov, A.,
- 480 Baltensperger, U., Barmet, P., Benduhn, F., Bianchi, F., Breitenlechner, M., Clarke, A., Curtius, J., Dommen, J., Donahue, N.
- 481 M., Ehrhart, S., Flagan, R. C., Franchin, A., Guida, R., Hakala, J., Hansel, A., Heinritzi, M., Jokinen, T., Kangasluoma, J.,
- 482 Kirkby, J., Kulmala, M., Kupc, A., Lawler, M. J., Lehtipalo, K., Makhmutov, V., Mann, G., Mathot, S., Merikanto, J.,
- Miettinen, P., Nenes, A., Onnela, A., Rap, A., Reddington, C. L. S., Riccobono, F., Richards, N. A. D., Rissanen, M. P.,
- Rondo, L., Sarnela, N., Schobesberger, S., Sengupta, K., Simon, M., Sipila, M., Smith, J. N., Stozkhov, Y., Tome, A., Trostl,
- J., Wagner, P. E., Wimmer, D., Winkler, P. M., Worsnop, D. R., and Carslaw, K. S.: Global atmospheric particle formation
- 486 from CERN CLOUD measurements, Science, 354, 1119-1124, 10.1126/science.aaf2649, 2016.
- Duplissy, J., Merikanto, J., Franchin, A., Tsagkogeorgas, G., Kangasluoma, J., Wimmer, D., Vuollekoski, H., Schobesberger,
- 488 S., Lehtipalo, K., and Flagan, R.: Effect of ions on sulfuric acid water binary particle formation: 2. Experimental data and
- 489 comparison with QC normalized classical nucleation theory, Journal of Geophysical Research: Atmospheres, 121,
- 490 1752-1775, 2016.
- Ehn, M., Kleist, E., Junninen, H., Petäjä, T., Lönn, G., Schobesberger, S., Maso, M. D., Trimborn, A., Kulmala, M., and
- Worsnop, D.: Gas phase formation of extremely oxidized pinene reaction products in chamber and ambient air, Atmos Chem
- 493 Phys, 12, 5113-5127, 2012.
- Ehn, M., Thornton, J. A., Kleist, E., Sipila, M., Junninen, H., Pullinen, I., Springer, M., Rubach, F., Tillmann, R., Lee, B.,
- Lopez-Hilfiker, F., Andres, S., Acir, I.-H., Rissanen, M., Jokinen, T., Schobesberger, S., Kangasluoma, J., Kontkanen, J.,
- 496 Nieminen, T., Kurtén, T., Nielsen, L. B., Jorgensen, S., Kjaergaard, H. G., Canagaratna, M., Dal Maso, M., Berndt, T., Petaja,
- 497 T., Wahner, A., Kerminen, V.-M., Kulmala, M., Worsnop, D. R., Wildt, J., and Mentel, T. F.: A large source of low-volatility
- 498 secondary organic aerosol, Nature, 506, 476-+, 10.1038/nature13032, 2014.

- 499 Eisele, F. L., and Tanner, D. J.: Measurement of the gas-phas concentration of H2SO4 and methane sulfonic-acid and
- estimates of H2SO4 production and loss in the atmosphere, J Geophys Res-Atmos, 98, 9001-9010, 10.1029/93jd00031,
- 501 1993.
- 502 Frege, C., Ortega, I. K., Rissanen, M. P., Praplan, A. P., Steiner, G., Heinritzi, M., Ahonen, L., Amorim, A., Bernhammer,
- 503 A.-K., and Bianchi, F.: Influence of temperature on the molecular composition of ions and charged clusters during pure
- biogenic nucleation, Atmos Chem Phys, 18, 65-79, 2018.
- Hamed, A., Korhonen, H., Sihto, S. L., Joutsensaari, J., Järvinen, H., Petäjä, T., Arnold, F., Nieminen, T., Kulmala, M., and
- 506 Smith, J. N.: The role of relative humidity in continental new particle formation, Journal of Geophysical Research:
- 507 Atmospheres, 116, 2011.
- Hanson, D., McMurry, P., Jiang, J., Tanner, D., and Huey, L.: Ambient pressure proton transfer mass spectrometry: detection
- of amines and ammonia, Environ Sci Technol, 45, 8881-8888, 2011.
- Hoffmann, T., O'Dowd, C. D., and Seinfeld, J. H.: Iodine oxide homogeneous nucleation: An explanation for coastal new
- particle production, Geophys Res Lett, 28, 1949-1952, 2001.
- Hyttinen, N., Kupiainen-Määttä, O., Rissanen, M. P., Muuronen, M., Ehn, M., and Kurtén, T.: Modeling the charging of
- 513 highly oxidized cyclohexene ozonolysis products using nitrate-based chemical ionization, The Journal of Physical Chemistry
- 514 A, 119, 6339-6345, 2015.
- Hyvönen, S., Junninen, H., Laakso, L., Maso, M. D., Grönholm, T., Bonn, B., Keronen, P., Aalto, P., Hiltunen, V., and Pohja,
- T.: A look at aerosol formation using data mining techniques, Atmos Chem Phys, 5, 3345-3356, 2005.
- Isaacman-VanWertz, G., Massoli, P., O'Brien, R., Lim, C., Franklin, J. P., Moss, J. A., Hunter, J. F., Nowak, J. B.,
- 518 Canagaratna, M. R., and Misztal, P. K.: Chemical evolution of atmospheric organic carbon over multiple generations of
- oxidation, Nature chemistry, 1, 2018.
- Johnson, D., and Marston, G.: The gas-phase ozonolysis of unsaturated volatile organic compounds in the troposphere,
- 521 Chemical Society Reviews, 37, 699-716, 2008.
- Jokinen, T., Sipila, M., Junninen, H., Ehn, M., Lonn, G., Hakala, J., Petaja, T., Mauldin, R. L., Kulmala, M., and Worsnop, D.
- 523 R.: Atmospheric sulphuric acid and neutral cluster measurements using CI-APi-TOF, Atmos Chem Phys, 12, 4117-4125,
- 524 2012.
- Jokinen, T., Sipilä, M., Richters, S., Kerminen, V. M., Paasonen, P., Stratmann, F., Worsnop, D., Kulmala, M., Ehn, M., and
- 526 Herrmann, H.: Rapid autoxidation forms highly oxidized RO2 radicals in the atmosphere, Angewandte Chemie International
- 527 Edition, 53, 14596-14600, 2014.
- Jonsson, Å. M., Hallquist, M., and Ljungström, E.: Impact of humidity on the ozone initiated oxidation of limonene,
- 529 Δ3-carene, and α-pinene, Environ Sci Technol, 40, 188-194, 2006.
- Jonsson, Å. M., Hallquist, M., and Ljungström, E.: Influence of OH scavenger on the water effect on secondary organic
- aerosol formation from ozonolysis of limonene, Δ3-carene, and α-pinene, Environ Sci Technol, 42, 5938-5944, 2008.
- Junninen, H., Ehn, M., Petaja, T., Luosujarvi, L., Kotiaho, T., Kostiainen, R., Rohner, U., Gonin, M., Fuhrer, K., Kulmala,
- M., and Worsnop, D. R.: A high-resolution mass spectrometer to measure atmospheric ion composition, Atmos Meas Tech, 3,
- 534 1039-1053, 2010.
- Kamens, R., Jang, M., Chien, C.-J., and Leach, K.: Aerosol Formation from the Reaction of α-Pinene and Ozone Using a
- Gas-Phase Kinetics-Aerosol Partitioning Model, Environ Sci Technol, 33, 1430-1438, 10.1021/es980725r, 1999.
- Kroll, J. H., Donahue, N. M., Jimenez, J. L., Kessler, S. H., Canagaratna, M. R., Wilson, K. R., Altieri, K. E., Mazzoleni, L.
- R., Wozniak, A. S., Bluhm, H., Mysak, E. R., Smith, J. D., Kolb, C. E., and Worsnop, D. R.: Carbon oxidation state as a
- metric for describing the chemistry of atmospheric organic aerosol, Nature Chemistry, 3, 133-139, 10.1038/nchem.948,
- 540 2011.
- Kuang, C., McMurry, P. H., McCormick, A. V., and Eisele, F. L.: Dependence of nucleation rates on sulfuric acid vapor
- 542 concentration in diverse atmospheric locations, J Geophys Res, 113, 10.1029/2007jd009253, 2008.
- Kulmala, M., Dal Maso, M., Makela, J. M., Pirjola, L., Vakeva, M., Aalto, P., Miikkulainen, P., Hameri, K., and O'Dowd, C.

- 544 D.: On the formation, growth and composition of nucleation mode particles, Tellus B, 53, 479-490,
- 545 10.1034/j.1600-0889.2001.d01-33.x, 2001.
- 546 Kulmala, M., Vehkamäki, H., Petäjä, T., Dal Maso, M., Lauri, A., Kerminen, V. M., Birmili, W., and McMurry, P. H.:
- 547 Formation and growth rates of ultrafine atmospheric particles: a review of observations, J Aerosol Sci, 35, 143-176,
- 548 10.1016/j.jaerosci.2003.10.003, 2004.
- Kulmala, M., Petäjä, T., Ehn, M., Thornton, J., Sipilä, M., Worsnop, D., and Kerminen, V.-M.: Chemistry of atmospheric
- 550 nucleation: on the recent advances on precursor characterization and atmospheric cluster composition in connection with
- atmospheric new particle formation, Annual review of physical chemistry, 65, 21-37, 2014.
- 552 Kürten, A., Rondo, L., Ehrhart, S., and Curtius, J.: Calibration of a Chemical Ionization Mass Spectrometer for the
- Measurement of Gaseous Sulfuric Acid, J Phys Chem A, 116, 6375-6386, 2012.
- Kürten, A., Jokinen, T., Simon, M., Sipila, M., Sarnela, N., Junninen, H., Adamov, A., Almeida, J., Amorim, A., Bianchi, F.,
- 555 Breitenlechner, M., Dommen, J., Donahue, N. M., Duplissy, J., Ehrhart, S., Flagan, R. C., Franchin, A., Hakala, J., Hansel,
- 556 A., Heinritzi, M., Hutterli, M., Kangasluoma, J., Kirkby, J., Laaksonen, A., Lehtipalo, K., Leiminger, M., Makhmutov, V.,
- Mathot, S., Onnela, A., Petaja, T., Praplan, A. P., Riccobono, F., Rissanen, M. P., Rondo, L., Schobesberger, S., Seinfeld, J.
- H., Steiner, G., Tome, A., Troestl, J., Winkler, P. M., Williamson, C., Wimmer, D., Ye, P., Baltensperger, U., Carslaw, K. S.,
- 559 Kulmala, M., Worsnop, D. R., and Curtius, J.: Neutral molecular cluster formation of sulfuric acid-dimethylamine observed
- in real time under atmospheric conditions, P Natl Acad Sci USA, 111, 15019-15024, 10.1073/pnas.1404853111, 2014.
- Kürten, A., Bergen, A., Heinritzi, M., Leiminger, M., Lorenz, V., Piel, F., Simon, M., Sitals, R., Wagner, A. C., and Curtius, J.:
- 562 Observation of new particle formation and measurement of sulfuric acid, ammonia, amines and highly oxidized organic
- 563 molecules at a rural site in central Germany, Atmos Chem Phys, 16, 12793-12813, 10.5194/acp-16-12793-2016, 2016.
- Kurten, T., Rissanen, M. P., Mackeprang, K., Thornton, J. A., Hyttinen, N., Jorgensen, S., Ehn, M., and Kjaergaard, H. G.:
- 565 Computational Study of Hydrogen Shifts and Ring-Opening Mechanisms in alpha-Pinene Ozonolysis Products, J Phys Chem
- 566 A, 119, 11366-11375, 10.1021/acs.jpca.5b08948, 2015.
- 567 Kurtén, T., Tiusanen, K., Roldin, P., Rissanen, M., Luy, J.-N., Boy, M., Ehn, M., and Donahue, N.: α-Pinene Autoxidation
- 568 Products May Not Have Extremely Low Saturation Vapor Pressures Despite High O:C Ratios, The Journal of Physical
- 569 Chemistry A, 120, 2569-2582, 10.1021/acs.jpca.6b02196, 2016.
- 570 Lee, B. H., Lopez-Hilfiker, F. D., Mohr, C., Kurtén, T., Worsnop, D. R., and Thornton, J. A.: An iodide-adduct
- 571 high-resolution time-of-flight chemical-ionization mass spectrometer: Application to atmospheric inorganic and organic
- 572 compounds, Environ Sci Technol, 48, 6309-6317, 2014.
- 573 Li, Y., Poeschl, U., and Shiraiwa, M.: Molecular corridors and parameterizations of volatility in the chemical evolution of
- organic aerosols, Atmos Chem Phys, 16, 3327-3344, 10.5194/acp-16-3327-2016, 2016.
- Makkonen, R., Asmi, A., Kerminen, V. M., Boy, M., Arneth, A., Hari, P., and Kulmala, M.: Air pollution control and
- 576 decreasing new particle formation lead to strong climate warming, Atmos Chem Phys, 12, 1515-1524,
- 577 10.5194/acp-12-1515-2012, 2012.
- McVay, R. C., Zhang, X., Aumont, B., Valorso, R., Camredon, M., La, Y. S., Wennberg, P. O., and Seinfeld, J. H.: SOA
- 579 formation from the photooxidation of α-pinene: systematic exploration of the simulation of chamber data, Atmos Chem Phys,
- 580 16, 2785-2802, 2016.
- Merikanto, J., Spracklen, D., Mann, G., Pickering, S., and Carslaw, K.: Impact of nucleation on global CCN, Atmos Chem
- 582 Phys, 9, 8601-8616, 2009.
- Merikanto, J., Duplissy, J., Määttänen, A., Henschel, H., Donahue, N. M., Brus, D., Schobesberger, S., Kulmala, M., and
- Vehkamäki, H.: Effect of ions on sulfuric acid water binary particle formation: 1. Theory for kinetic and nucleation -
- 585 type particle formation and atmospheric implications, Journal of Geophysical Research: Atmospheres, 121, 1736-1751,
- 586 2016.
- Metzger, A., Verheggen, B., Dommen, J., Duplissy, J., Prevot, A. S., Weingartner, E., Riipinen, I., Kulmala, M., Spracklen, D.
- V., Carslaw, K. S., and Baltensperger, U.: Evidence for the role of organics in aerosol particle formation under atmospheric

- 589 conditions, Proc Natl Acad Sci U S A, 107, 6646-6651, 10.1073/pnas.0911330107, 2010.
- Molteni, U., Bianchi, F., Klein, F., Haddad, I. E., Frege, C., Rossi, M. J., Dommen, J., and Baltensperger, U.: Formation of
- highly oxygenated organic molecules from aromatic compounds, Atmos Chem Phys, 18, 1909-1921, 2018.
- 592 Napari, I., Noppel, M., Vehkamäki, H., and Kulmala, M.: Parametrization of ternary nucleation rates for H2SO4 NH3 -
- 593 H2O vapors, Journal of Geophysical Research: Atmospheres, 107, 2002.
- 594 O'Dowd, C. D., Geever, M., Hill, M. K., Smith, M. H., and Jennings, S. G.: New particle formation: Nucleation rates and
- 595 spatial scales in the clean marine coastal environment, Geophys Res Lett, 25, 1661-1664, 1998.
- Ortega, I. K., Donahue, N. M., Kurtén, T., Kulmala, M., Focsa, C., and Vehkamaki, H.: Can Highly Oxidized Organics
- 597 Contribute to Atmospheric New Particle Formation?, J Phys Chem A, 120, 1452-1458, 10.1021/acs.jpca.5b07427, 2016.
- 598 Pankow, J. F., and Asher, W. E.: SIMPOL. 1: a simple group contribution method for predicting vapor pressures and
- enthalpies of vaporization of multifunctional organic compounds, Atmos Chem Phys, 8, 2773-2796, 2008.
- 600 Poschl, U., Martin, S. T., Sinha, B., Chen, O., Gunthe, S. S., Huffman, J. A., Borrmann, S., Farmer, D. K., Garland, R. M.,
- 601 Helas, G., Jimenez, J. L., King, S. M., Manzi, A., Mikhailov, E., Pauliquevis, T., Petters, M. D., Prenni, A. J., Roldin, P.,
- 602 Rose, D., Schneider, J., Su, H., Zorn, S. R., Artaxo, P., and Andreae, M. O.: Rainforest Aerosols as Biogenic Nuclei of
- Clouds and Precipitation in the Amazon, Science, 329, 1513-1516, 2010.
- Rissanen, M. P., Kurtén, T., Sipilä, M., Thornton, J. A., Kausiala, O., Garmash, O., Kjaergaard, H. G., Petäjä, T., Worsnop, D.
- R., and Ehn, M.: Effects of chemical complexity on the autoxidation mechanisms of endocyclic alkene ozonolysis products:
- 606 From methylcyclohexenes toward understanding α-pinene, The Journal of Physical Chemistry A, 119, 4633-4650, 2015.
- 607 Schobesberger, S., Junninen, H., Bianchi, F., Lonn, G., Ehn, M., Lehtipalo, K., Dommen, J., Ehrhart, S., Ortega, I. K.,
- 608 Franchin, A., Nieminen, T., Riccobono, F., Hutterli, M., Duplissy, J., Almeida, J., Amorim, A., Breitenlechner, M., Downard,
- 609 A. J., Dunne, E. M., Flagan, R. C., Kajos, M., Keskinen, H., Kirkby, J., Kupc, A., Kürten, A., Kurtén, T., Laaksonen, A.,
- Mathot, S., Onnela, A., Praplan, A. P., Rondo, L., Santos, F. D., Schallhart, S., Schnitzhofer, R., Sipila, M., Tome, A.,
- Tsagkogeorgas, G., Vehkamaki, H., Wimmer, D., Baltensperger, U., Carslaw, K. S., Curtius, J., Hansel, A., Petaja, T.,
- Kulmala, M., Donahue, N. M., and Worsnop, D. R.: Molecular understanding of atmospheric particle formation from sulfuric
- 613 acid and large oxidized organic molecules, Proc Natl Acad Sci U S A, 110, 17223-17228, 10.1073/pnas.1306973110, 2013.
- Shen, X. J., Sun, J. Y., Zhang, Y. M., Wehner, B., Nowak, A., Tuch, T., Zhang, X. C., Wang, T. T., Zhou, H. G., Zhang, X. L.,
- Dong, F., Birmili, W., and Wiedensohler, A.: First long-term study of particle number size distributions and new particle
- formation events of regional aerosol in the North China Plain, Atmos Chem Phys, 11, 1565-1580, 10.5194/acp-11-1565-2011,
- 617 2011.
- 618 Sihto, S.-L., Kulmala, M., Kerminen, V.-M., Maso, M. D., Petäjä, T., Riipinen, I., Korhonen, H., Arnold, F., Janson, R., and
- Boy, M.: Atmospheric sulphuric acid and aerosol formation: implications from atmospheric measurements for nucleation and
- early growth mechanisms, Atmos Chem Phys, 6, 4079-4091, 2006.
- Thomson, B., and Iribarne, J.: Field induced ion evaporation from liquid surfaces at atmospheric pressure, The Journal of
- 622 Chemical Physics, 71, 4451-4463, 1979.
- Tobias, H. J., Docherty, K. S., Beving, D. E., and Ziemann, P. J.: Effect of relative humidity on the chemical composition of
- secondary organic aerosol formed from reactions of 1-tetradecene and O3, Environ Sci Technol, 34, 2116-2125, 2000.
- Tobias, H. J., and Ziemann, P. J.: Kinetics of the gas-phase reactions of alcohols, aldehydes, carboxylic acids, and water with
- the C13 stabilized Criegee intermediate formed from ozonolysis of 1-tetradecene, The Journal of Physical Chemistry A, 105,
- 627 6129-6135, 2001.
- Tröstl, J., Chuang, W. K., Gordon, H., Heinritzi, M., Yan, C., Molteni, U., Ahlm, L., Frege, C., Bianchi, F., and Wagner, R.:
- The role of low-volatility organic compounds in initial particle growth in the atmosphere, Nature, 533, 527-531, 2016.
- Vehkamäki, H., and Riipinen, I.: Thermodynamics and kinetics of atmospheric aerosol particle formation and growth,
- 631 Chemical Society Reviews, 41, 5160-5173, 2012.
- Weber, R., Marti, J., McMurry, P., Eisele, F., Tanner, D., and Jefferson, A.: Measurements of new particle formation and
- ultrafine particle growth rates at a clean continental site, Journal of Geophysical Research: Atmospheres, 102, 4375-4385,

634 1997.

- Weber, R., McMurry, P. H., Mauldin, R., Tanner, D., Eisele, F., Clarke, A., and Kapustin, V.: New particle formation in the
- remote troposphere: A comparison of observations at various sites, Geophys Res Lett, 26, 307-310, 1999.
- Yu, H., McGraw, R., and Lee, S.-H.: Effects of amines on formation of sub-3 nm particles and their subsequent growth,
- 638 Geophys Res Lett, 39, 10.1029/2011gl050099, 2012.
- Zhang, R., Khalizov, A., Wang, L., Hu, M., and Xu, W.: Nucleation and growth of nanoparticles in the atmosphere, Chem
- 640 Rev, 112, 1957-2011, 10.1021/cr2001756, 2012.
- Zhang, X., McVay, R. C., Huang, D. D., Dalleska, N. F., Aumont, B., Flagan, R. C., and Seinfeld, J. H.: Formation and
- 642 evolution of molecular products in α-pinene secondary organic aerosol, Proceedings of the National Academy of Sciences,
- 643 112, 14168-14173, 2015.
- Zhao, J., Khalizov, A., Zhang, R., and McGraw, R.: Hydrogen-bonding interaction in molecular complexes and clusters of
- aerosol nucleation precursors, The Journal of Physical Chemistry A, 113, 680-689, 2009.
- Zhao, J., Eisele, F. L., Titcombe, M., Kuang, C., and McMurry, P. H.: Chemical ionization mass spectrometric measurements
- of atmospheric neutral clusters using the cluster CIMS, Journal of Geophysical Research: Atmospheres, 115, 2010.
- Zhao, J., Ortega, J., Chen, M., and Mcmurry, P. H.: Dependence of particle nucleation and growth on high molecular weight
- 649 gas phase products during ozonolysis of α-pinene, Atmospheric Chemistry & Physics, 13, 7631-7644, 2013.

Table 1. Experiment conditions and products.

651

654

655656

Precursor	Exp (#)	Monoterpene (ppbv)	O ₃ (ppbv)	Cyclo-hexane (ppmv)	Initial rate ¹ (10 ⁸ molecules cm ⁻³ s ⁻¹)	O ₃ consumption ² (ppb)	SOA ³ (μg m ⁻³)
Limonene	1	1085	900±10	0	1410	159-166	138-208
	2	1085	900±10	217	1410	139-150	81-147
	3	54	350±5	0	27.3	34-41	0
α-pinene	4	1111	900±10	0	625	103-110	761-1042
	5	1111	900±10	222	625	93-102	414-735
	6	54	350±5	0	11.8	23-30	0
\triangle^3 -carene	7	1111	900±10	0	267	72-89	55-93
	8	1111	900±10	222	267	70-86	34-92
	9	54	350±5	0	5.05	11-16	0

^{652 &}lt;sup>1</sup>At room temperature (298K), the rate coefficients for limonene, α-pinene and Δ³-carene to react with O₃ were 200×10⁻¹⁸, 653 86.6×10⁻¹⁸, 37×10⁻¹⁸ cm³ molecule⁻¹ s⁻¹, respectively.

²O₃ consumption values were calculated from the difference between inlet and outlet O₃ concentrations.

³SOA mass concentrations were calculated from SMPS-measured volume concentrations and an assumed organic effective density (1.2 g cm⁻³).

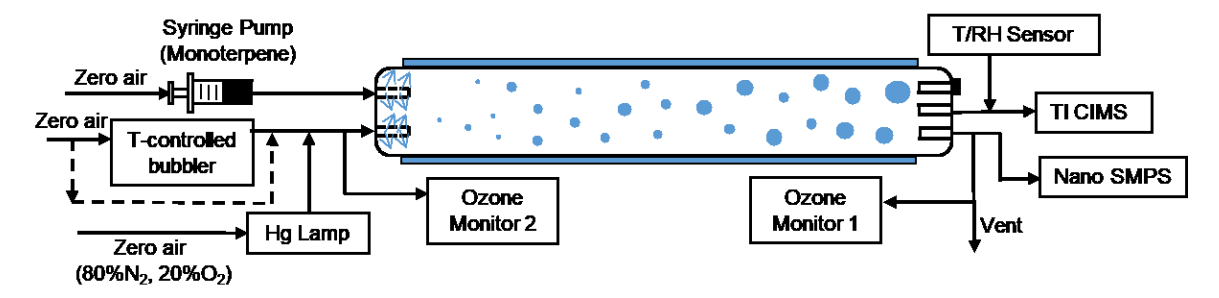


Figure 1. Experiment setup for the flow tube experiments. The 8.5 L flow tube was placed at a temperature-controlled room (21±1°C) and covered. The total flowrate was 8.5 LPM. The RH was adjusted by mixing temperature controlled bubbler flow with dry zero air.

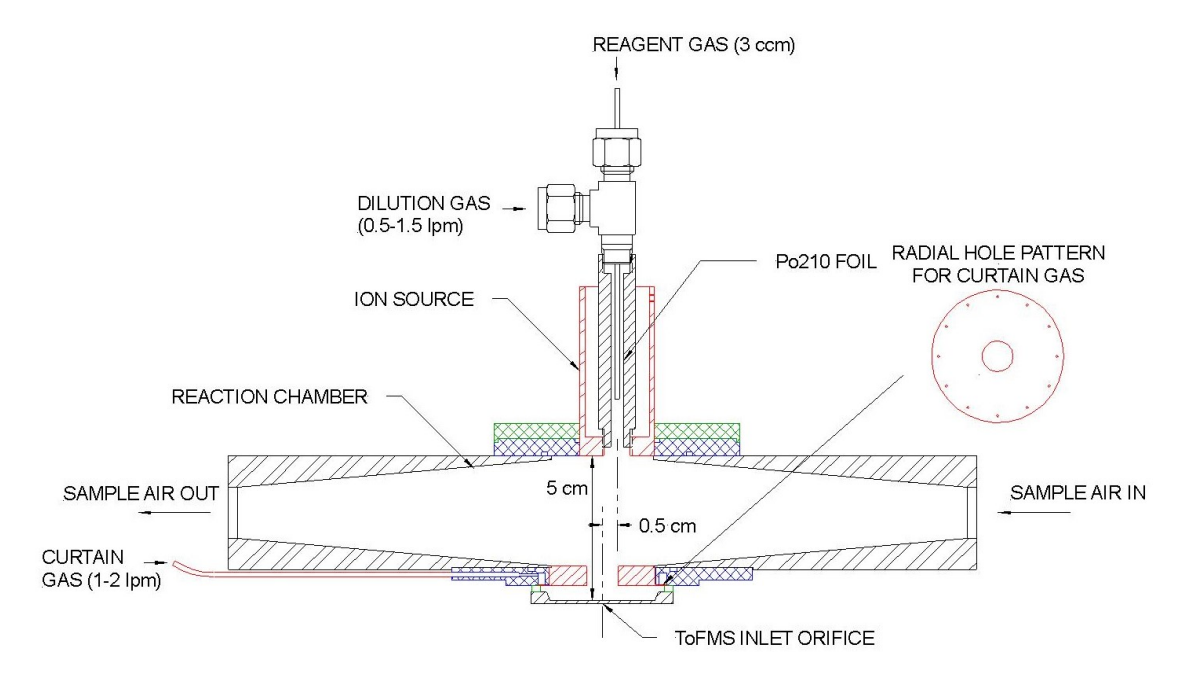


Figure 2. Schematic of the transverse ionization (TI) inlet, showing the N_2 curtain gas configuration. The relative position of the ion source to the inlet orifice is adjustable. The configuration shown here is the most sensitive in calibrations with H_2SO_4 (see Section 3.1).

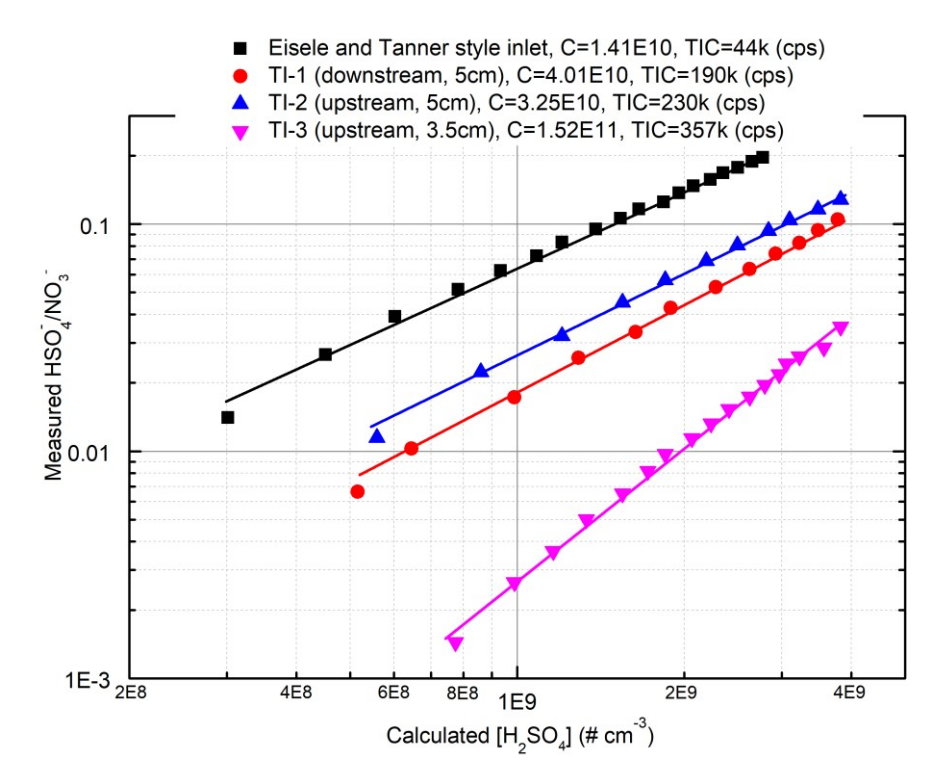


Figure 3. Comparison of the sensitivities for the two inlets to H₂SO₄. The calibration process followed that reported by Kürten et al. (2012) and is discussed in detail in the supplementary material. TI-1, 2, 3 represent different locations of the ion source relative to the inlet orifice of the mass spectrometer. "upstream" and "downstream" indicated 0.5 cm upstream or downstream along the sample flow axis and "3.5 cm" and "5 cm" indicate 3.5 or 5 cm away from the inlet orifice along the reagent ion flow axis.

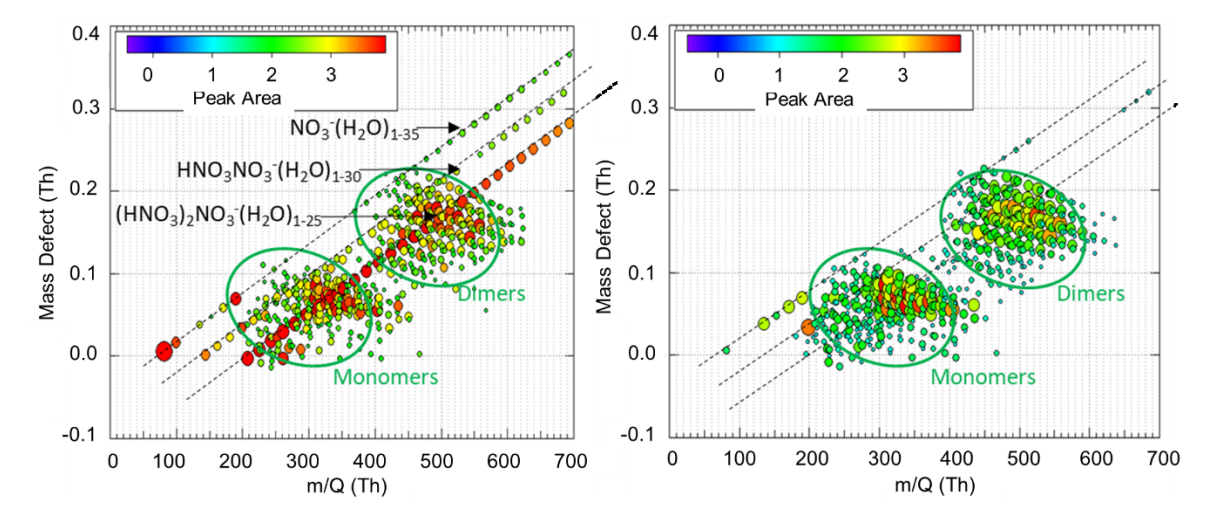


Figure 4. Mass defect plots of α -pinene ozonolysis HOMs with 0 LPM (left) and 1 LPM (right) N_2 curtain gas flow when RH \approx 85%, with monomer and dimer HOMs circled in green. The most intense ions comprising 60% of the total ion count are plotted for clarity. H_2O clusters $(H_2O)_m(HNO_3)_nNO_3^-$ (m = 1 - 35, n = 0 - 2) are circled in red in the left plot and are notably absent with the application of the N_2 curtain gas. $(HNO_3)_2NO_3^-$ and $HNO_3NO_3^-$ are much more likely to cluster with H_2O than NO_3^- .

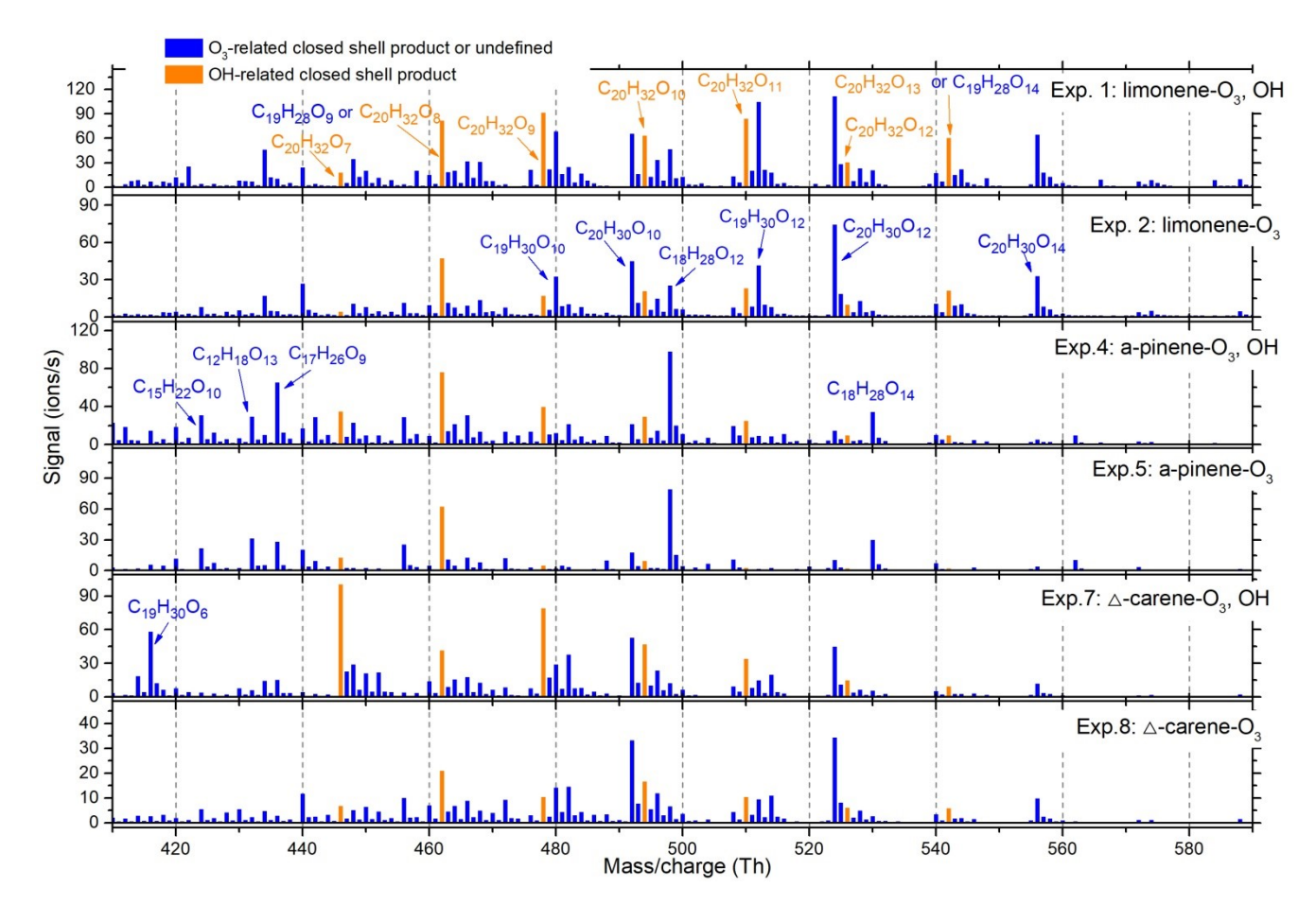


Figure 5. Average dimer mass spectrum in each of the particle generation experiments. The OH- and O_3 -derived species were distinguished by comparing relative abundance of experiments with and without OH scavenger. All the peaks shown were in the form of adducts with NO_3 or HNO_3NO_3 reagent ions.

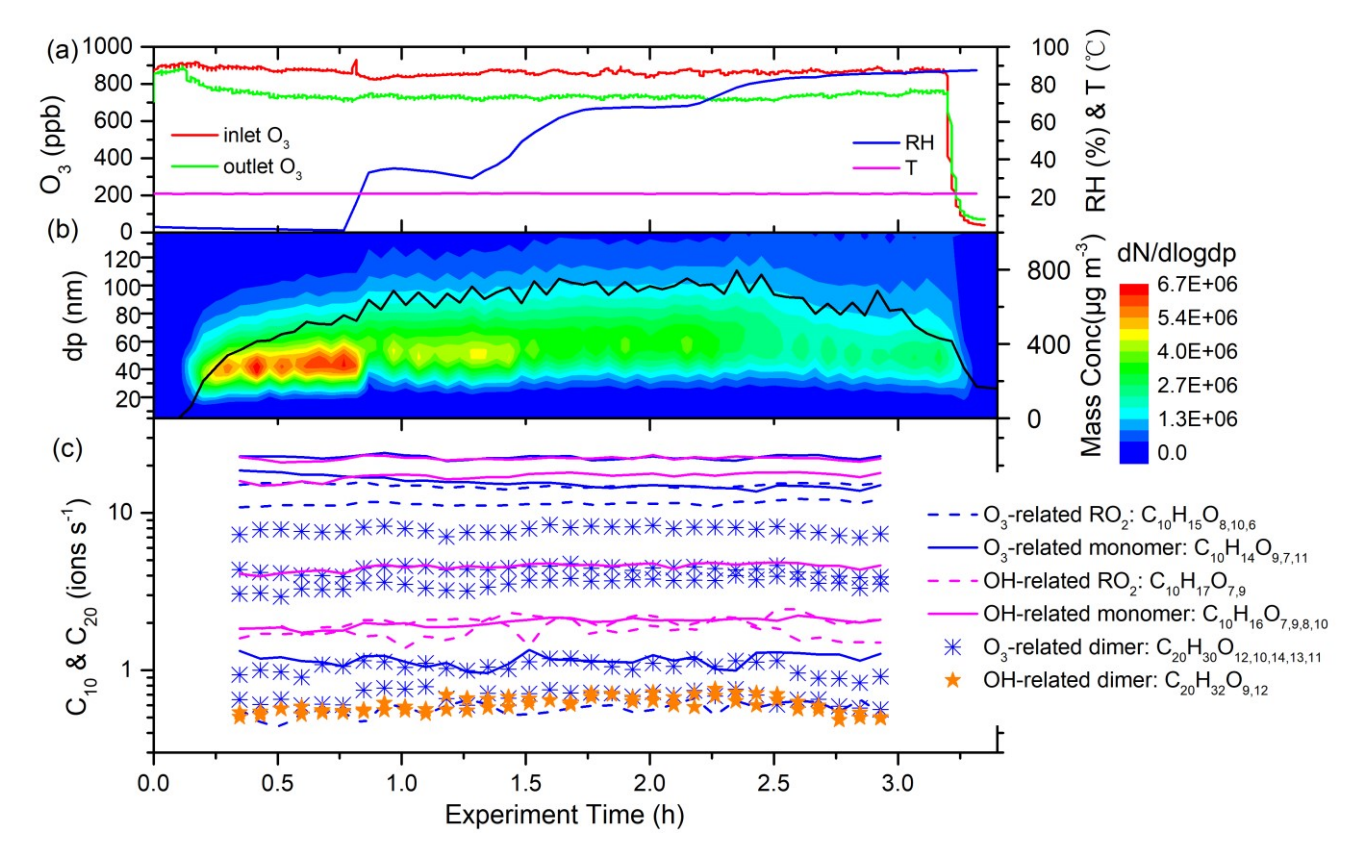


Figure 6. Time series of experimental parameters, particle size distribution, and key ions during EXP. 2 (limonene oxidized by O₃ without OH scavenger). (a) inlet and outlet O₃ concentrations, temperature, and RH; (b) Particle size distribution and integrated mass concentrations (assuming effective density is 1.2 g cm⁻³); (c) Some of the main HOMs detected by TI-CIMS with NO₃⁻ reagent ion. The subscript oxygen numbers in the formulae were ranked (left-to-right) according to signal abundance of the corresponding molecule.

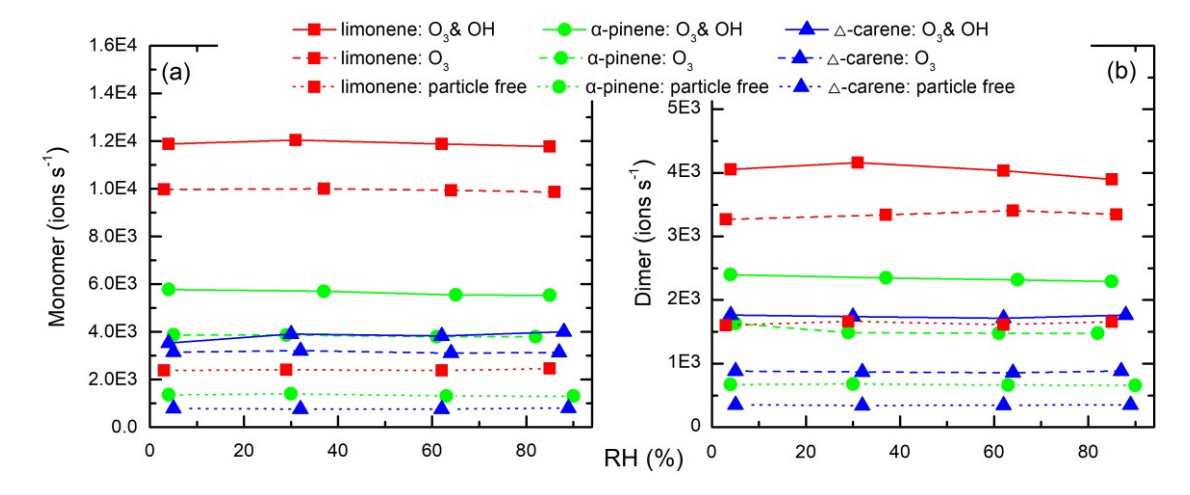


Figure 7. Average (a) monomer and (b) dimer HOMs signal intensity (ions s^{-1}) as a function of RH in each experiment. Monomer signals were the sum of $C_{5^{-10}}$ molecules and dimer signals were the sum of $C_{15^{-20}}$ molecules. No obvious signal change was seen for increasing RH in any of the experiments.

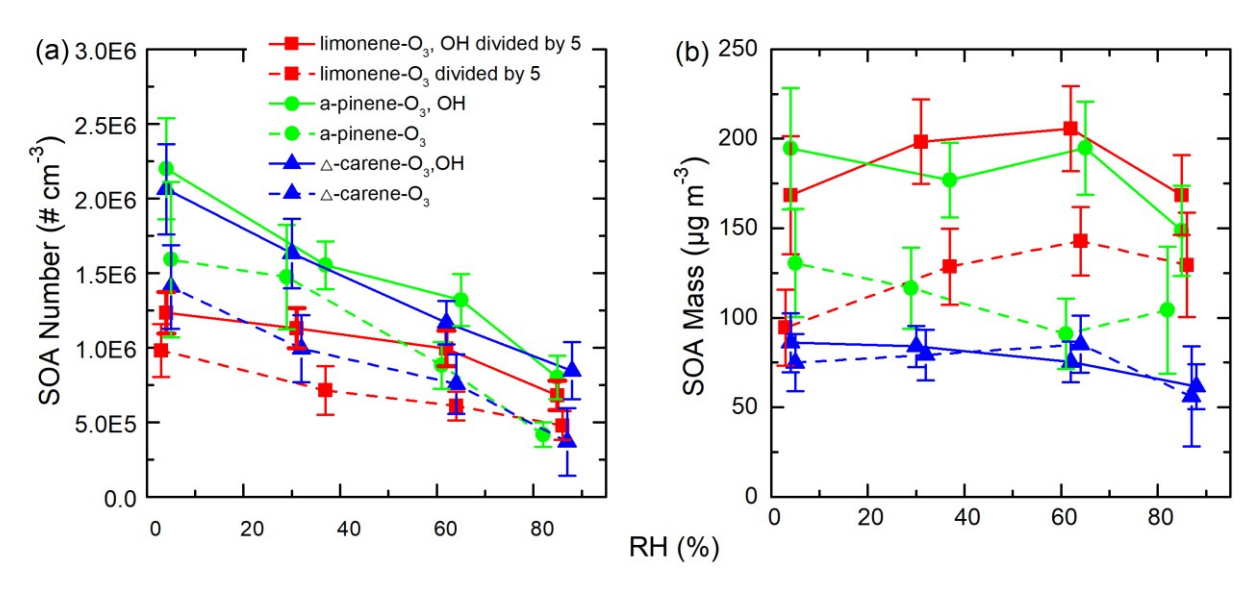


Figure 8. SOA (a) number and (b) mass concentrations as a function of RH during different experiments. The error bars were calculated using both the statistical errors of all individual size distributions during each RH stage and assuming a systematic CPC counting error of 10%).

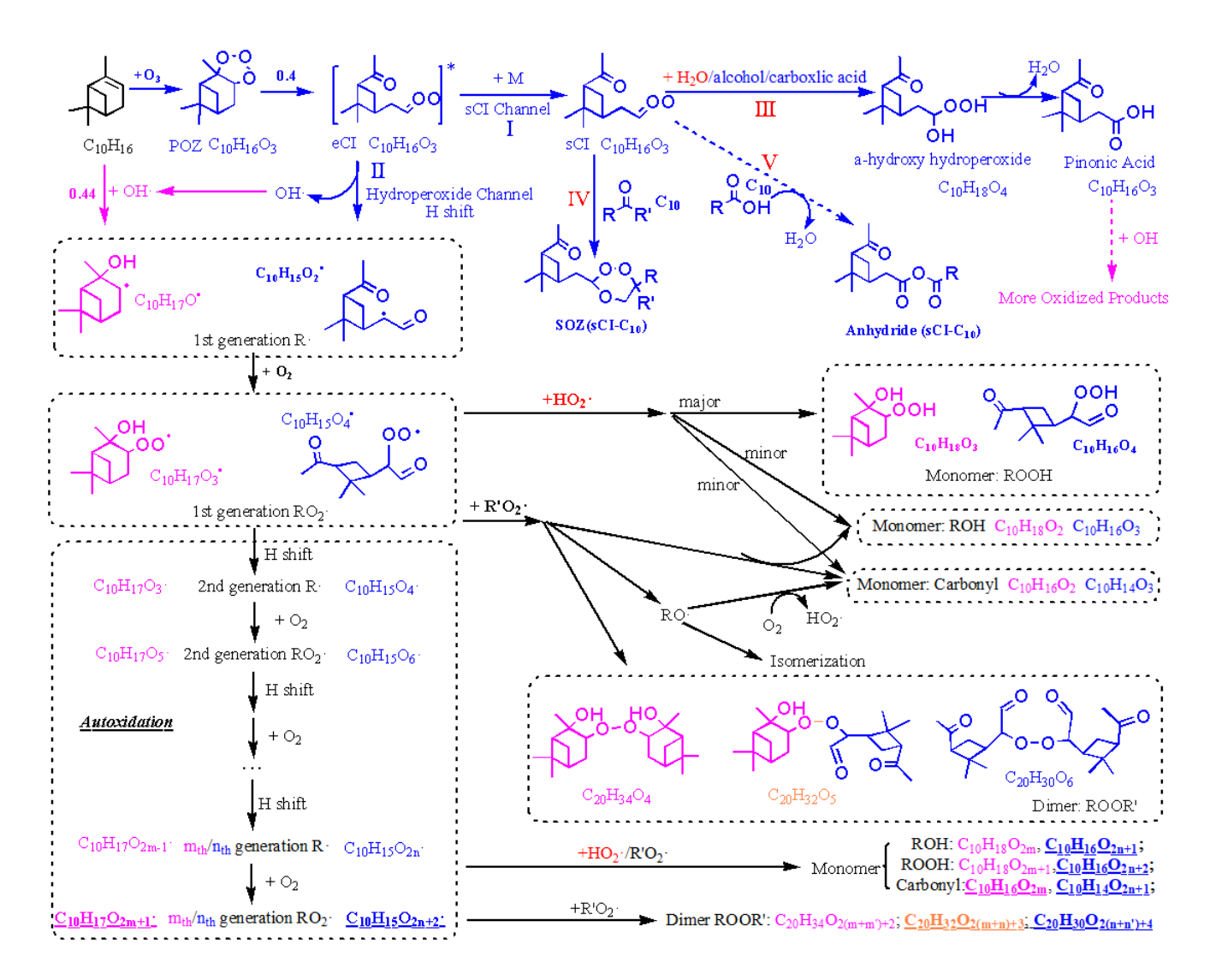


Figure 9. Proposed key steps in the formation of the representative C_{10} and C_{20} closed shell products from α -pinene oxidation and possible water vapor influence. Dashed lines represent pathways that may or may not happen, depending on the situation. Pink and blue colors represented the pathways or products from O_3 and OH oxidation, respectively. Common pathways or products are indicated in black type. Orange colors represented the combined products of O_3 and OH chemistry. Red colors highlight the direct or indirect influence of water. Underlined formulae were the main products observed from the mass spectrum. $C_{10}H_{18}O_{2m}$ and $C_{20}H_{34}O_{2(m+m')}$ were not observed in our spectrum, but they dominated the spectrum in other reported experiments where extra OH was generated (Berndt et al., 2016).

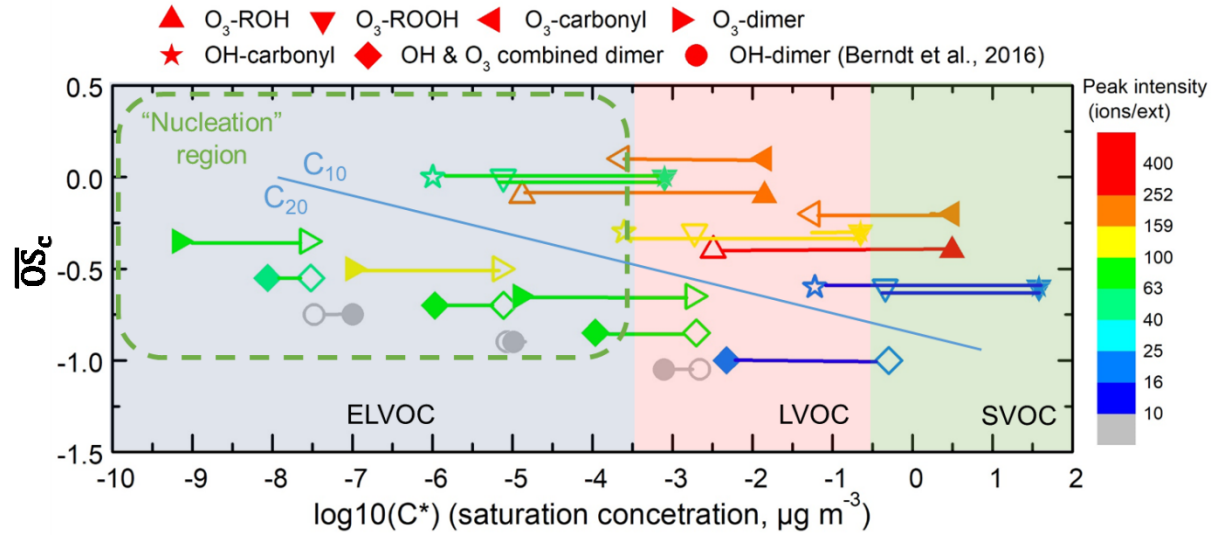


Figure 10. Vapor saturation mass concentration C^* (T=298 K) of the major C_{10} and C_{20} closed shell products were predicted with SIMPOL.1 (open points) (Pankow and Asher, 2008) and Molecular Corridor method (filled points) (Li et al., 2016). Lines connecting the open points and filled points represent the difference between the two methods. O_3 or OH-derived, monomers and dimers are presented in different shapes. The peak intensity, represented by color, is from Exp.1 (limonene oxidation without OH scavenger). The gray points, which represent OH-derived dimers, are dominating products in OH initiated oxidation experiments (Berndt et al., 2016) while not observed in this study. Data used in this figure are given in Table S1. The nucleation region (green dashed rectangle) is from Donahue et al. (2013).